Miniature Ferroelectret Microphone Design and Performance Evaluation Using Laser Excitation

Linas Svilainis, *Senior Member, IEEE*, Andrius Chaziachmetovas, *Member, IEEE*, Valdas Eidukynas, Tomás Gómez Álvarez-Arenas, *Member, IEEE*, and Steve Dixon

***Abstract*— Miniature microphones suitable for measurements of ultrasonic wave field scans in air are expensive or lack sensitivity or do not cover the range beyond 100 kHz. It is essential that they are too large for such fields measurements. The use of a ferroelectret (FE) film is proposed to construct a miniature, needle-style 0.5-mm-diameter sensitive element ultrasonic microphone. FE has an acoustic impedance much closer to that of air compared with other alternatives and is low cost and easy to process. The performance of the microphone was evaluated by measuring the sensitivity area map, directivity, ac response, and calibrating the absolute sensitivity. Another novel contribution here is that the sensitivity map was obtained by scanning the focused beam of a laser diode over the microphone surface, producing thermoelastic ultrasound excitation. The electroacoustic response of the microphone served as a sensitivity indicator at a scan spot. Micrometer scale granularity of the FE sensitivity was revealed in the sensitivity map images. It was also demonstrated that the relative ac response of the microphone can be obtained using pulsed laser beam thermoelastic excitation of the whole microphone surface with a laser diode. The absolute sensitivity calibration was done using the hybrid three-transducer reciprocity technique. A large aperture, air coupled transducer beam was focused onto the microphone surface, using the parabolic off-axis mirror. This measurement validated the laser ac response measurements. The FE microphone performance was compared with biaxially stretched polyvinylidene difluoride (PVDF) microphone of the same construction.**

***Index Terms*— Air coupled ultrasound, ferroelectret (FE) film, laser ultrasound, ultrasonic needle microphone.**

Manuscript received 12 September 2022; accepted 1 November 2022. Date of publication 4 November 2022; date of current version 28 November 2022. This work was supported by the European Regional Development Fund under Project 01.2.2-LMT-K-718-03-0026 through grant agreement with the Research Council of Lithuania (LMTLT). *(Corresponding author: Linas Svilainis.)*

Linas Svilainis and Andrius Chaziachmetovas are with the Electronics Engineering Department, Kaunas University of Technology, LT-51368 Kaunas, Lithuania (e-mail: linas.svilainis@ktu.lt; andrius.chaziachmetovas@ktu.lt).

Valdas Eidukynas is with the Department of Mechanical Engineering and Design, Kaunas University of Technology, LT-51368 Kaunas, Lithuania (e-mail: valdas.eidukynas@ktu.lt).

Tomás Gómez Álvarez-Arenas is with the Institute for Physical and Information Technologies, Spanish National Research Council, 28006 Madrid, Spain (e-mail: t.gomez@csic.es).

Steve Dixon is with the Department of Physics, University of Warwick, CV4 7AL Coventry, U.K. (e-mail: s.m.dixon@warwick.ac.uk).

Digital Object Identifier 10.1109/TUFFC.2022.3220082

I. Introduction

MANY applications, such as local positioning systems, ranging, obstacle avoidance, anemometry, or nondestructive testing (NDT), utilize air-coupled ultrasound. Air-coupled ultrasound applications call for efficient signal transduction, due to the high acoustic impedance mismatch between the air and the samples of interests. Therefore, most effort is usually concentrated on transducer development. A necessary measurement in transducer development is the directivity and acoustic field distribution [1], [2], [3], [4], [5], [6], [7], [8], [9], [10], [11]. A ball reflector is used for such measurements, if only the pulse-echo directivity is required [5], [6]. A small size receiver is used for the field distribution measurements. The size of the sensing element of the receiver should be less than the wavelength of twice the central frequency of the probe under test, but not less than 0.5 mm [6]. However, there are no ultrasonic range microphones of this size available. The most frequently used type of microphone is the 1/8 in (3.18-mm diameter)-type 4138 microphone from Brüel & Kjær (Nærum, Denmark) [2], [3], [4], [10], [11]. Unfortunately, its bandwidth is limited to 140 kHz [1], and its relatively large size means that it is only really useful up to 50 kHz, if spatial averaging effects are to be avoided [6], [7], [8], [9]. Most microphones are intended for applications that are not required to go beyond 100 kHz. In addition, sensitivity decreases with the frequency, and it is often difficult to avoid the appearance of resonances that destroy the expected flat response of the microphone. These include resonances in the structure of the microphone and even resonances in the sensing material. Another alternative microphone design is the polyvinylidene difluoride (PVDF) membrane hydrophone, whose active area diameter can be down to 0.5 mm [12]. It has a wide, uniform frequency response from 100 kHz up to 5 MHz, but the device diameter including the frame is 60 mm. The PVDF membrane also has to be perforated around the sensing area, in order to avoid Lamb wave generation on the membrane. Another widely used alternative is the miniature piezoceramic disk "pinducer" [3], [4] (for example, the VP-1093 from the Valpey-Fisher Corporation), which has a diameter of 1.35 mm. Though the acoustic impedance of the PVDF membrane is an order of magnitude lower than the piezoceramic in the pinducer, the pinducer is often preferable given its greater piezoelectric sensitivity and improved directional response.

The PVDF needle hydrophones, despite being intended for use in water, can also be considered, but as with pinducers, they have a large impedance mismatch to air, so that the sensitivity for a 0.5-mm hydrophone is 0.8 μV/Pa [59]. Placing an aperture in front of the receiver can attain a 1-mm-diameter sensing area [13], but the parasitic capacitance remains high, so sensitivity is low. Optical ultrasound microphones can be divided into four categories: 1) the Fabry–Perot resonator [15] at the end of an optical fiber; 2) the distributed Bragg reflector (DBR) [16], [25] at the end of the optical fiber; 3) the ring resonator coupled to the optical fiber or waveguide [14], [24]; and 4) refraction index modulation-based sensors [18], [19], [20]. The interferometric cavity microphone (based on refraction index modulation) commercially available from XARION Laser Acoustics has a sensing aperture of 2.0 × 0.3 mm [18]. Another simple approach is to use a pellicle and laser vibrometer to detect displacement of the pellicle [58]. While offering wide bandwidth and a small sensitive area size (e.g., Fabry–Perot interferometer-based FOHSv2, commercially available from Precision Acoustics Ltd. [17]), this type of sensor requires an additional light-processing engine, and the whole system can be expensive. Micromachined (MEMS) air-coupled ultrasonic sensors [21], [22], [23], [26], [27] can have the sensitive element sizes of 0.1 mm [21]. The appearance of novel applications in the field of consumer electronics and the use of MEMS microphones [23] is extending this range up to 200 kHz. Although it is crucial for the study of higher frequency ultrasonic air-coupled ultrasonic transducers used in NDT, there is still little interest in these novel applications for further increasing this frequency range. Finally, the MEMS devices need intricate chip fabrication technology, and their structure can be extremely fragile. Commercially available MEMS-based microphones can operate up to the frequencies of 80 kHz [39].

To conclude, there are no suitable, inexpensive, microphones less than 3-mm diameter available for ad hoc measurements and scans of ultrasonic fields in air. The current options that are available are either expensive (optical microphones are 10k USD order, and hydrophones 1k USD), or lack sensitivity due to an impedance mismatch to air, or are large or do not cover the frequency range beyond 100 kHz. The key challenges are the size (0.5-mm diameter), sensitivity, and cost.

The ferroelectret (FE) is one of the recently proposed materials for ultrasound transmission and detection [28], [29], [30], [31], [32], [33], [34]. While the piezoelectric strain constant d_{33} for PVDF is around 20 pC/N, d_{33} for FE devices range from 25 to 700 pC/N, with new developments reaching 1200 pC/N [34] or even 1400 pC/N [35]. The FE devices have a lower density of around 330–530 kg/m^3 and a lower speed of sound in the material of 85–177 m/s, resulting in an acoustic impedance that is much closer to that of air when compared with other alternatives 0.028–0.056 MRayl [31], [32], [33]. The FE material is low cost, is readily commercially available, and usually comes with one side metalized. It is bonded to a rigid backing, so that it operates by compressing in its thickness direction, rather than via a flexing mechanism. The properties of the FE material can also be further improved by additional processing [38]. There have been reports [36], [37] of applications using FE sensors, but of 5- × 5-mm size, with a sensitivity of 2 mV/Pa and a bandwidth of only 10 kHz.

Fig. 1. Microphone construction (left) and the assembled device (right).

Here, we report the design of a small, 0.5-mm diameter, FE-based microphone, operating in the 150–450-kHz frequency range. Construction is very simple and mainly involves adhesively bonding the FE film onto the end of the semirigid coaxial cable. Material and labor cost are minimal. A similar construction of microphone was produced using PVDF, for comparison purposes. The sensitive area size was measured using focused laser ultrasound with μm resolution. Absolute sensitivity and ac response were measured in the 150–450-kHz frequency range, using a hybrid three-transducer reciprocity technique [59]. Relative ac response was measured using wide beam laser ultrasound.

II. Microphone Design

A schematic of the FE microphone's construction and a photograph of the assembled device are presented in Fig. 1. The 70-μm-thick EMFIT film HS-03-20BRAL1 (from EMFIT Ltd., Vaajakoski, Finland) was used in this microphone design. The film was adhesively bonded (using MB295 from Master Bond, Hackensack, NJ, USA) onto the end of 15-mm-long, 2.159-mm-diameter, RG405-type, semirigid coaxial cable (from Belden, Inc., St. Louis, MO, USA). The other end of the semirigid cable was soldered into an SMA connector (2911-40024 type, from Amphenol, Wallingford, CT, USA). The EMFIT film comes with one side already metalized, which faced outward and served as ground electrical connection. Connection to the cable shield was made using silver conductive paint (SCP03B from Electrolube, Leicestershire, U.K.). The center conductor (0.5-mm diameter) of the coaxial cable served as the "live" electrode for the FE film.

The output of the microphone was directly connected to a 40-dB preamplifier (SE-RX01-02), which was designed and manufactured by the Kaunas University of Technology (KTU). The preamplifier input impedance was 5 kΩ, and the lower passband frequency was 90 kHz, with an additional third-order Butterworth filter limiting the upper passband frequency to 3 MHz. More details on the preamplifier design and noise performance can be found in [41].

The PVDF-based hydrophone was manufactured using the same construction as the FE microphone. A biaxially stretched 50-μm-thick PVDF film (from Piezotech Arkema-CRRA, Pierre-Benite Cedex, France) was used. The PVDF film was supplied with metallization on both sides, so one electrode was etched out.

TABLE I
PROPERTIES OF THE FE FILM USED FOR MICROPHONE DESIGN

Material	h, μm	ρ, kg/m^3	$f_{rez\lambda/4}$,MHz	c, m/s	d_{33}, pC/N
FE	70	530	0.32	90	80
PVDF	40	1780	14	2200	25

In both cases, PVDF and FE, the vibrational mode of the sensor is the thickness mode, and thickness is much smaller than the lateral dimension. Moreover, in the case of the FE material, the large anisotropy grants a large decoupling between thickness and lateral vibration modes. The microscopic scale simulation, presented in [28], confirms that the simple thickness resonance calculation is sufficient for ac response estimation. Material properties (thickness h, density ρ, propagation velocity c, and quasi-static piezoelectric coefficient d_{33}) and the expected $\lambda/4$ resonance frequency (the backing is copper, high impedance) are listed in Table I.

The bandwidth used in the investigation was set to 150–450 kHz ($\pm 50\%$ f_{rez}), which was limited by the resonance frequency of the FE microphone.

III. PERFORMANCE EVALUATION

The size of the "live" electrode (0.5-mm-diameter center conductor of the coaxial cable) is intended to define the size of the sensitive area of the microphone. Nevertheless, experiments were set to evaluate the active area size of the microphone, as pressure waves incident to the side of the central reason could, in principle, yield a response.

A. Sensitive Area Size Evaluation Using Laser Ultrasound

The evaluation of the size of the sensitive area size can be performed using a focused transducer, scanning over the probe's surface [42], [43]. However, the focused probe's beam should be 50-μm diameter or smaller, in order to scan the 0.5-mm-diameter area. Focusing an air-coupled ultrasonic transducer to such a small size would be challenging, not least because the ultrasonic wavelength is almost 2.2 mm at 150 kHz. A reasonable alternative approach seems to be using a laser ultrasound source [44], which can be directly coupled to the surface of the test sample. The acoustic contact is stable, there is no need for immersion, impedance mismatch does not affect the signal level, and there is no reverberation in the coupling media. It can also be focused to a small size, with a laser spot of 50-μm diameter being attainable. It is important that such a source is not resonant, and the pulsed laser beam can provide wideband excitation with an arbitrary source shape, using suitable optics [45].

The thermoelastic regime (power density below the damage threshold of the test material) [46] was used. In this case, the thermal expansion of the volume heated by laser pulse is the major source of the ultrasound.

Pulsed laser diodes are now commercially available at a reasonable cost, and the planned application will send series of pulses. The laser drivers required to do this are not currently commercially available, but the development of such a laser driver has been reported [48]. However, the laser diode used in [48] has a highly asymmetric beam shape: the laser aperture size is 225 × 10 μm. This is an inherent property of >10-W laser diodes, because they are edge-emitting devices. The 10-μm dimension is too small, and a large portion of acoustic energy is converted into other modes, and only a small amount is directed normal to the surface. The 225-μm dimension is really too wide to scan an area of 500-μm diameter. Therefore, a different laser diode type with an aperture size of 85 × 10 μm was used (905D1S3J03UA type, 27 W at 11 A from Laser Components, Olching, Germany).

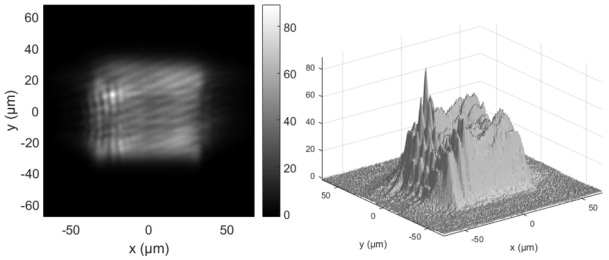

Fig. 2. Laser beam profile in 2-D (left) and 3-D (right) 250 μm away from focus.

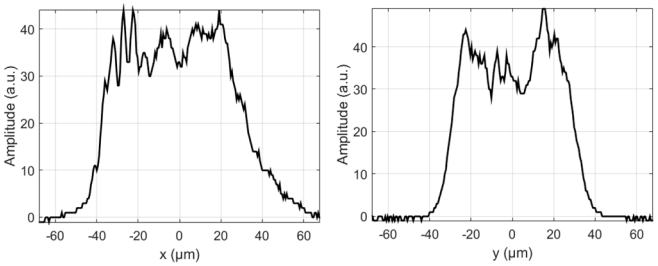

Fig. 3. Beam profile along x (left) and y (right) 250 μm further from focus.

However, the abovementioned modification was not sufficient for scanning requirements: the beam shape at focus was still asymmetric, and edge-emitting lasers also have inherent astigmatism [51], [52] (virtual emission origins for slow and fast axes do not match). Usually, a dedicated lens system is designed to solve this issue [51], [52], [53], or a complex optical system, including cylindrical lenses [54] or a pair of anamorphic prisms, is used [55]. The case presented here used a simpler approach: instead of correcting the astigmatism, it was exploited. Due to astigmatism, when the fast axis is focused, the slow axis is slightly defocused, so it is blurred. But 250 μm further from the laser from this focus point, the slow axis gets focused, and the fast axis starts to be blurred (Figs. 2 and 3), which yields a symmetric beam shape at this point.

The laser beam can be made smaller using different lens combinations, but a smaller beam has a lower portion of pressure directed normal to the surface [45], [46], [47]. Then, in order to have an acceptable acoustic output, laser power has to be increased, and the sample surface is potentially damaged due to the increased power density of the beam.

A larger beam size also has a lower power density, so that the danger of ablative surface damage is reduced. A beam

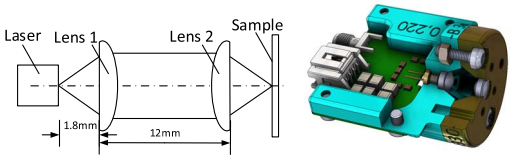

Fig. 4. Lens system (left) and assembled laser probe (right) drawing.

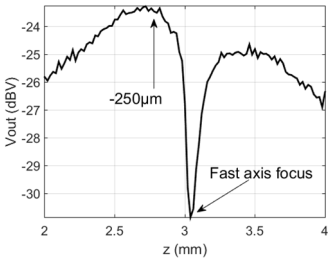

Fig. 5. Acoustic signal intensity versus distance from lens.

size of 60 × 60 μm was found to be optimal, for a balance between resolution and acoustic output. A simple two identical lens (3.1-mm effective focal length, 354330-B type, Thorlabs Inc., NJ, USA) 1:1 magnification system was sufficient to focus the laser beam onto the sample surface. The whole laser excitation system (Fig. 4: laser driver with current monitor, lens system, and encapsulation) design is quite compact, at 40 × 40 × 25 mm.

It is easy to position the beam on the sample surface along the z-axis: there is a dip in the acoustic response (see Fig. 5). The dip occurs due to the narrow laser beam: focusing creates the point-like source, and there is less pressure produced normal to the surface [45], [46], [47].

The amplitude of the acoustic pressure produced is proportional to the energy absorbed from the laser beam [47]. The microphone's outer surface has an aluminum coating (Fig. 1), which reflects a large portion of incident laser energy.

Another problem is that the thermoelastic regime laser ultrasound is plagued by the production of a dual acoustic pulse: a laser generated heat pulse produces two acoustic pulses traveling in opposite directions: toward the material bulk and outward [49]. The second pulse is immediately reflected back into the material, and, if laser penetration depth is small, it cancels the first one. Therefore, generation of the longitudinal waves normal to the material surface is complicated in the thermoelastic regime. However, there is a solution: if a second pulse is either delayed or canceled, the longitudinal wave normal to the surface is enhanced by several orders of magnitude [46], [47], [48], [49]. The application of a thin laser energy absorbing layer provides a similar result [60], [61], [62]. Therefore, the microphone surface was spray-coated with a high-temperature paint (800 °C BOKSC263206-type from Bostik SA, Colombes, France). The presence of the coating also improves the acoustic pressure produced, due to improved energy absorption, and it also reduces the amplitude of the surface wave [50]. Two thicknesses of the coating layer were used: thin (single, brief spray, microphones EMFIT-M1, and PVDF) and thick (two, long

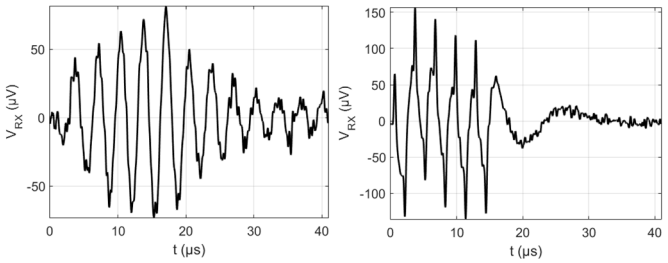

Fig. 6. FE (left) and PVDF-based (right) microphone response to laser excitation.

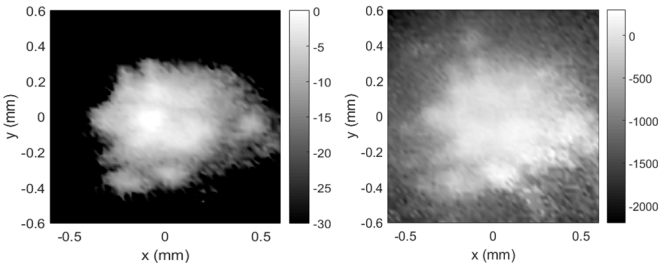

Fig. 7. C-scan of signal amplitude (left—gray scale is dB) and phase (right—gray scale is ns) of microphone EMFIT-M1 (thin light-absorbing coating).

sprays, and microphone EMFIT-P). One would expect that the thick coating had better absorption, but any additional mass on the EMFIT material will alter its acoustic properties. Thin coating should have less influence.

The laser probe was mounted on a kinematic tilt stage and was attached to a 3-D positioning system [57]. The laser was driven by 300 kHz, five periods, and the rectangular current tone bursts of 2 A. Such current corresponds to 5-W laser output pulse trains. Adjustment along the z-axis was done at a reduced 1-A current. An example of the received voltage response to laser excitation for the FE and PVDF-based microphone is presented in Fig. 6.

An in-house designed ultrasonic data acquisition system was used to drive the laser probe (100-MHz sampling frequency binary coded sets), to digitize the preamplifier output (10-bit, 100-MHz sampling frequency) and to control the 3-D positioning (10-μm resolution for x- and y-axes, and 5-μm resolution for the z-axis) [57].

The amplitude and phase of the received signal were estimated using the sine wave correlation (SWC) technique [56]. The SWC can be interpreted as a continuous time Fourier transform at single frequency or as a lock-in amplifier. Because of its narrow bandwidth, it can deliver high SNR and is immune to front ringing caused by the signal's rectangular envelope. The signal was gated by selecting the part of the signal where envelope has reached half of its maximum.

The C-scan image of the 1200- × 1200-μm scan over the FE microphone surface with a thin coating at a 10-μm step is presented in Fig. 7 (left: amplitude and right: phase as delay). Phase information was used to gate out the surface waves (equivalent to a 400-ns wide gate placed at 400-ns delay). The corresponding beam profile cross section is shown in Fig. 8.

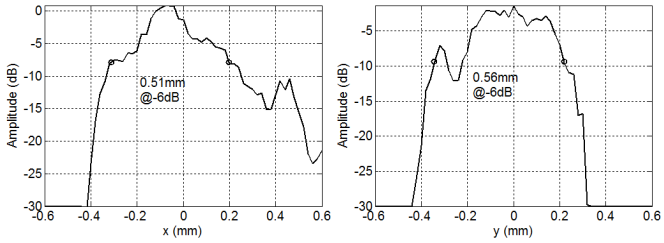

Fig. 8. Beam profile cross section along *x*-axis (left) and *y*-axis (right) for microphone EMFIT-M1 (thin light-absorbing coating).

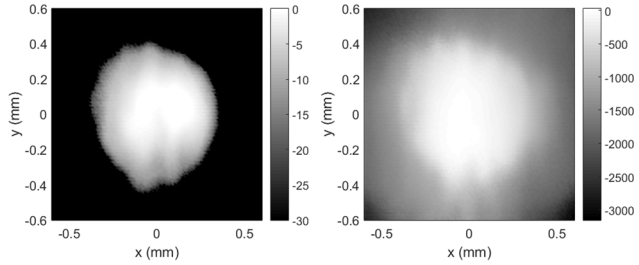

Fig. 9. C-scan of signal amplitude (left—gray scale is dB) and phase (right—gray scale is ns) of microphone EMFIT-P (thick light-absorbing coating).

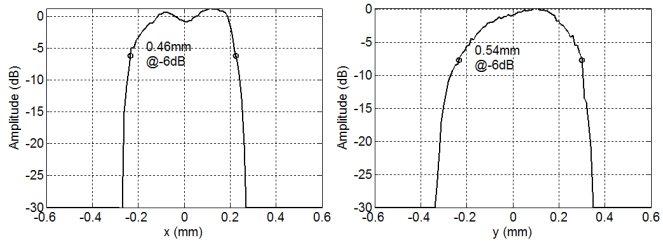

Fig. 10. Beam profile cross section along *x*-axis (left) and *y*-axis (right) for microphone EMFIT-P (thick light-absorbing coating).

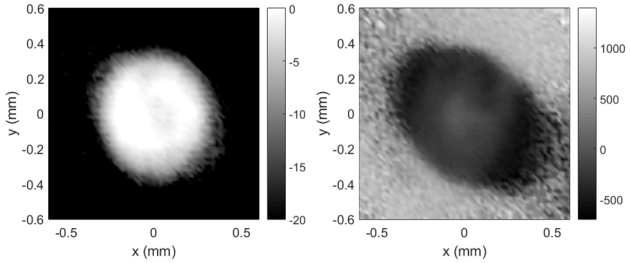

Fig. 11. C-scan of signal amplitude (left—gray scale is dB) and phase (right—gray scale is ns) of PVDF microphone (thin light-absorbing coating).

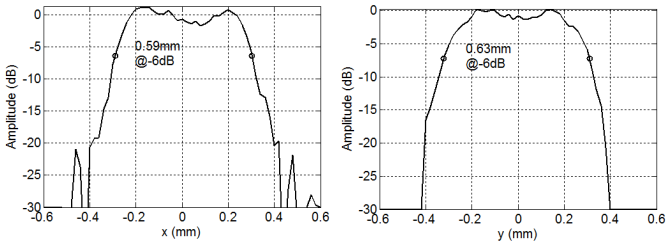

Fig. 12. Beam profile cross section along *x*-axis (left) and *y*-axis (right) for PVDF microphone (thin light-absorbing coating).

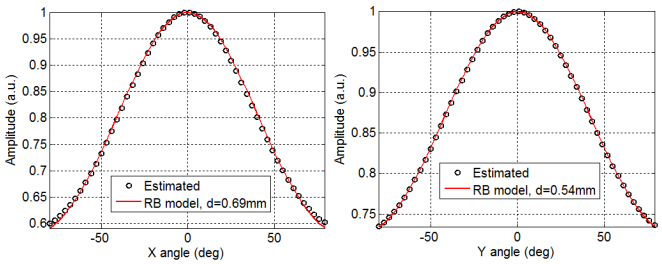

Fig. 13. Microphone EMFIT-M1 directivity along *x*-axis (left) and *y*-axis (right).

The −6-dB sizing approach was used for sensitive area size estimation. The sensitive area size of the EMFIT-M1 microphone is 0.51 × 0.56 mm, which is slightly wider than the electrode diameter of 0.5 mm. It should be noted that the sensitivity map of this microphone is nonuniform. This is expected, since the FE film contains voids with trapped charge, the lateral size of which varies from few to hundreds of μm [32].

The sensitivity map of the FE microphone with the thick coating is presented in Fig. 9, and the corresponding beam profile cross section is shown in Fig. 10.

The thick coating added some smoothing, and the beam profile is more uniform here. The beam size is larger than expected: 0.46 × 0.54 mm. Again, phase information was used to gate out the surface waves, which arrive later.

The sensitivity map of the PVDF-based microphone with the thin absorbing coating is presented in Fig. 11, and the corresponding beam profile cross section is shown in Fig. 12.

The sensitivity map of the PVDF version of the microphone is very smooth, with well-defined edges. The PVDF material is uniform, so the sensitivity map is uniform too. The beam size is larger than expected: 0.59 × 0.63 mm, instead of the expected 0.5-mm diameter of the electrode.

B. Sensitive Area Size Evaluation Using Directivity

Evaluation of the sensitive area size is usually done using a directivity measurement of the hydrophone microphone [63]. Such a measurement is not possible in this case: measurement should be done in the far-field, and as the transducer has large aperture, the distance should be large, 200 mm [67]. Air nonlinearity [65] and attenuation effects will be very strong.

Nevertheless, information for the directivity estimation is already available as a sensitivity map. The sensitivity value was taken from the amplitude of the sinusoidal signal. The x and y coordinates on the sensitivity map and the observation angle were used to calculate the sinusoid phase at a 25.4-mm distance. All signals were summed up for every observation angle (angle varied with 3° step in −80° to +80° range), and the corresponding directivity was obtained. The estimated directivity plots (circles) for the microphones are presented in Fig. 13 (EMFIT-M1), Fig. 14 (EMFIT-P), and Fig. 15 (PVDF).

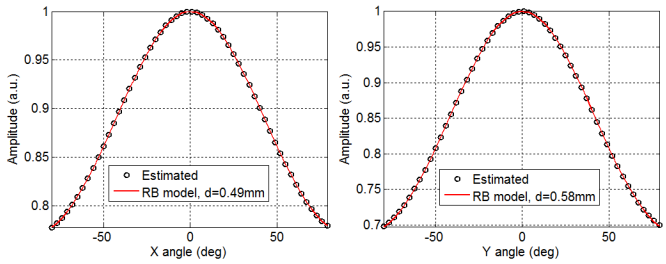

Fig. 14. Microphone EMFIT-P directivity along *x*-axis (left) and *y*-axis (right).

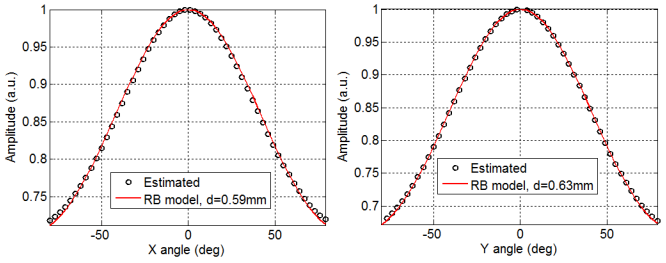

Fig. 15. Microphone PVDF directivity along *x*-axis (left) and *y*-axis (right).

TABLE II
MICROPHONE SENSITIVE AREA SIZE ESTIMATION RESULTS

Estimation	-6dB sizing		Directivity fit RB model	
Microphone	*x*, mm	*y*, mm	*x*, mm	*y*, mm
EMFIT-M	0.51	0.56	0.69	0.54
EMFIT-P	0.46	0.54	0.49	0.58
PVDF	0.59	0.63	0.59	0.63

The estimated directivity was then approximated (red solid line in Figs. 13–15) by a circular piston in a rigid planar baffle (RB) function [8]

$$D_{\mathrm{RB}}(k,a,\theta)=\frac{2J(k\cdot a\cdot\sin(\theta))}{k\cdot a\cdot\sin(\theta)} \tag{1}$$

where θ is the observation angle, a is the microphone effective radius, $k=2\pi/\lambda$ is the wavenumber, $\lambda=c/f$ is the wavelength in air, c is the ultrasound propagation velocity in air, and f is the frequency at which the directivity estimation was done.

The results of the size estimation of the sensitive element for both techniques are summarized in Table II.

For the EMFIT-M1 microphone, the size of the sensitive element along the x-axis was estimated correctly from the directivity estimation, but the -6-dB sizing (laser scan) returned a different value. It might look as though the estimated size along the x-axis was smaller for the laser scan, but by looking at Fig. 8 (left), one can see the reason for the underestimation was the presence of a small peak at -0.1 mm. Otherwise, the element size would have been around 0.65 mm. The rest of the measurements (EMFIT-M1 along y, EMFIT-P, and PVDF microphones) produced matching results for both evaluation techniques.

It can be concluded that the sensitivity map produced by laser excitation provides valuable information for the reliable estimation of the size of the sensitive element, and can replace the directivity measurement according to [63]. Furthermore, the directivity measurement requires precise beam location on the microphone tip and distance tracking. Laser scanning requires less adjustment.

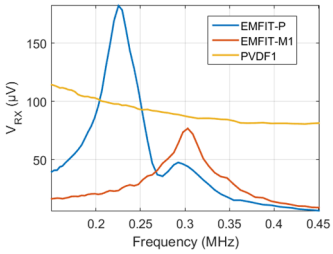

Fig. 16. Relative ac response of all microphones obtained by laser excitation.

C. AC Response Evaluation Using Laser Ultrasound

A thermoelastic laser generated ultrasound can also be used for microphone ac response evaluation. While the absolute measurements are complicated, the relationship between different frequency components can be obtained reliably. The laser modulation used a rectangular 4-A, 100-μs duration tone burst, with a variable frequency (150–450-kHz range). The amplitude of the microphone response was extracted using SWC [56]. In order to get an integral response of the whole microphone surface, and to amplify the longitudinal wave normal to the microphone surface, a wide beam was required (comparable to the 0.5-mm diameter of the microphone sensitive area). A vertical-cavity surface-emitting laser (VCSEL) array laser diode was used (1.2- $\times$ 1-mm emitting surface, V107C021A-940 from OSRAM). The laser beam was focused onto the microphone surface using a two lens system, with a magnification of 0.5, which resulted in a beam size of 0.6 $\times$ 0.5 mm. The signal amplitudes at the amplifier input for 4-A laser excitation are presented in Fig. 16.

It can be seen that the FE film (EMFIT label) and the PVDF-based microphones produced comparable output signals. The FE microphone with the thick coating (EMFIT-P) had a larger amplitude response than either the FE or the PVDF microphones coated by a thin absorber layer. It is notable that the PVDF has a much broader ac response bandwidth than the FE, since its sensing element through-thickness resonance is located at 14 MHz (Table I).

The measured ac response was also used to estimate the absorbing coating thickness from the resonant frequency shift for the EMFIT material [33]. The coating material density was estimated to be 800 kg/m^3. The thin coating layer (EMFIT-M) produced a 6% resonance frequency shift, which corresponds to a 5-μm coating thickness. The thick coating (EMFIT-P) produced a 30% resonance shift, which corresponds to a 26-μm coating thickness.

D. AC Response Evaluation Using Reciprocity Calibration

Modification of the three-transducer reciprocity [63] sensitivity calibration was proposed in [59]. The same idea

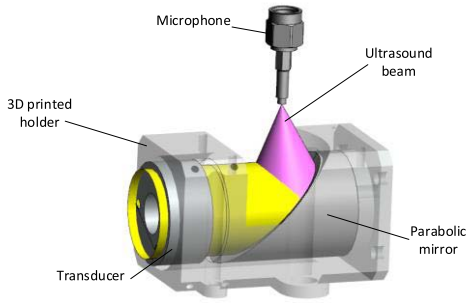

Fig. 17. Parabolic off-axis mirror focusing holder 3-D drawing.

was used here to evaluate the microphone ac response. The modified technique uses a large aperture transducer, mounted on a parabolic mirror holder, and an off-axis mirror (14OAP-1-25-90-AL type from Standa Photonics) to focus the beam onto the microphone (Fig. 17).

The setup involves two of the same type of transducers, which are assumed to be reciprocal. The electrical transfer impedance was measured in four configurations: transducer–transducer (Z_{12}), no focusing at a distance of 25.4 mm (near field), and transducer–microphone (Z_{1M} and Z_{2M}) at a focal distance (25.4 mm)

$$Z_{12} = \frac{E_{RX2}}{I_{TX1}}, \quad Z_{1M} = \frac{E_{RXM1}}{I_{TX1}}, \quad Z_{2M} = \frac{E_{RXM2}}{I_{TX2}} \tag{2}$$

where I_{TX1} and I_{TX2} are the input currents for transmitting transducers 1 and 2, respectively, E_{RX2} is the receiving transducer 2 output voltage, and E_{RXM1} and E_{RXM2} are the output voltages of the microphone, for a signal received from transducers 1 and 2, respectively.

The transducers used were designed and manufactured by the Spanish National Research Council (CSIC) and contain a 20-mm-diameter piezoelectric element. More details on the transducer design can be found in [64]. With this setup, the calibration can be done in very a confined space. For comparison, the measurement distance should be 917 mm for a 20-mm-diameter piezoelectric element at 300 kHz, according to [63]. It is essential that the use of the focused source minimizes frequency-dependent diffraction effects [66]. Air attenuation and nonlinearity effects [65] are minimized because of the short propagation distance and low-amplitude excitation signals. The transmitting transducer was excited using the half-bridge topology pulser SE-TX01-02 [68], using bipolar ±5-V rectangular, 0.15–0.45-MHz frequency, and 100-μs duration toneburst pulses. The low excitation voltage also prevented the transducer from heating and, thus, signal distortions. Due to the small microphone size and the acoustic impedance mismatch to air, the signals detected had low SNR, and so were averaged 1000 times. The signal received by the microphone (black line in Fig. 18) was gated by selecting the part of the signal where the envelope was stable. The amplitude and phase of the received signal were estimated using the SWC technique (red line in Fig. 18) [56]. The results of Fig. 18 demonstrate that at 300 kHz, the FE response is ten times higher than that of the PVDF.

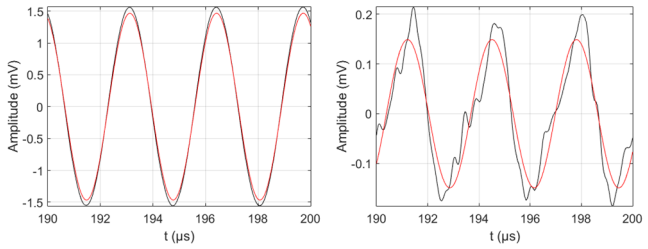

Fig. 18. Zoomed-in view on the signal received when excited by air-coupled transducer 300-kHz tone burst: FE (left) versus PVDF (right). Red is sinusoid with the amplitude and phase extracted using SWC, and black is raw signal.

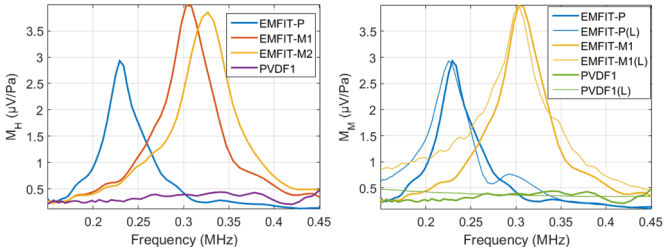

Fig. 19. Microphone ac response obtained by three-transducer reciprocity calibration (left) comparison with laser excitation (right).

The reception sensitivity of the microphone is [59]

$$M_M = \sqrt{\frac{2G_{TT}c \cdot d^2 Z_{1M} Z_{2M}}{A\rho f^2 Z_{12}}} \tag{3}$$

where G_{TT} is the diffraction correction factor for transducer–transducer propagation (obtained using the paraxial expansion described in [28]), ρ is the air density, A is the active surface area of the transducer, and d is the propagation distance.

Ultrasound attenuation in air was not accounted for, due to the short propagation distances. The expected focal spot size at 300 kHz is 1.7 mm, and the microphone's sensitive element diameter is 0.5 mm, and therefore, beam size correction was not necessary.

The results for all microphone measurements are presented in Fig. 19.

The laser measurement results [Fig. 19 (right), thin lines (L)] have been added for comparison with amplitude and are normalized to match the calibration results. It can be concluded that both laser excitation and reciprocity calibration produced similar ac responses. Laser excitation is not affected by air movement or air temperature influence on the propagation time.

The FE-based microphone has much better sensitivity at its first through thickness resonant frequency, compared with its PVDF-based counterpart. Performance beyond this resonance is comparable, for the case where a thin light-absorbing coating is used. A thick coating lowers the resonance frequency as expected and results in the sensitivity and bandwidth being reduced.

Due to the large impedance mismatch between the air and any solid material (in this case with PVDF and FF), the active film response is quite resonant (much more resonant than what can be observed in the case of hydrophones in water).

The location of the thickness resonance depends on the ultrasonic velocity in the film, the film thickness, and any additional load added to the film. It must be taken into account that both density and elastic constant of FF are very low, so the FF thickness resonance is very sensitive to any mass load added. The expected resonance of the FF film is about 320 kHz, which correspond well with the results from EMFIT-M1. EMFIT-P shows a resonance displaced to lower frequency (230 kHz), due to the additional mass of the thick coating added to the FF film. Precise and thin layer coating control, from spin coating, sputtering, or vacuum evaporation, can reduce this frequency drop compared with the uncoated device. However, it should be remembered that no coating would be required if there was no need to provide absorption of the incident laser beam. In the case of the PVDF sensor, the thickness resonance is expected to appear at 14 MHz (Table I), because the ultrasonic compression wave velocity in the PVDF is larger, and its thickness is smaller, and therefore, the PVDF response is quite flat. The PVDF is also more dense, so the additional coating used does not influence the frequency shift as much as for FE.

IV. Conclusion

It was demonstrated that a miniature, 0.5-mm-diameter microphone can be produced using the FE film. Production is simple and involves adhesively bonding the FE film on the end of the semirigid coaxial cable.

Another contribution proposed in this article is the sensitivity map measurement technique, which uses thermoelastic mode laser excitation. Excitation was accomplished by focusing the edge-emitting laser diode on microphone surface, attaining 60-μm resolution of the sensitivity map image. Defocusing and astigmatism were exploited usefully for laser beam profile symmetrization, resulting in a very simple lens system. The whole laser excitation system design is very compact, being 40 $\times$ 40 mm in size. It was demonstrated that the microphone has a sensitive area diameter slightly wider than the electrode diameter of 0.5 mm, which was also confirmed by estimating the microphone directivity from the sensitivity map. The estimated directivity matches the *Jinc* function, corresponding to a circular piston in an RB.

The absolute sensitivity and ac response were obtained by a three-transducer reciprocity calibration technique. The sensitivity measurement demonstrated that the FE microphone peak sensitivity is 4 μV/Pa, which is much higher than for the microphone made of PVDF. The sensitivity can be further enhanced, as the current device used FE materials with $d_{33} =$ 80 pC/N, but newer FE materials have $d_{33} = 1400$ pC/N [35]. Broader bandwidth and higher sensitivity can be achieved if such materials appear on the market.

One more novelty presented here is the microphone relative ac response measurement, using laser ultrasound. A medium power VCSEL array laser diode was used for thermoelastic excitation of the whole microphone surface.

Acknowledgment

The authors would like to thank A. Aleksandrovas and M. Varatinskas for their help in the preparation of experimental modules.

References

[1] *1/8-Inch Pressure-Field Microphone Type 4138*, Brüel & Kjær, Nærum, Denmark, 2021.

[2] R. J. Kazys, R. Sliteris, and J. Sestoke, "Air-coupled low frequency ultrasonic transducers and arrays with PMN-32%PT piezoelectric crystals," *Sensors*, vol. 17, no. 1, pp. 1–20, Jan. 2017, doi: 10.3390/s17010095.

[3] G. Benny and G. Hayward, "Beam profile measurements and simulations for air-coupled ultrasonic transducers," in *Proc. IEEE Ultrason. Symp.*, vol. 1, Oct. 1999, pp. 1041–1044.

[4] G. Benny, G. Hayward, and R. Chapman, "Beam profile measurements and simulations for ultrasonic transducers operating in air," *J. Acoust. Soc. Amer.*, vol. 107, no. 4, pp. 2089–2100, Apr. 2000, doi: 10.1121/1.428491.

[5] G. Allevato et al., "Real-time 3-D imaging using an air-coupled ultrasonic phased-array," *IEEE Trans. Ultrason., Ferroelectr., Freq. Control*, vol. 68, no. 3, pp. 796–806, Mar. 2021, doi: 10.1109/TUFFC.2020.3005292.

[6] *Non-Destructive Testing—Characterization and Verification of Ultrasonic Examination Equipment—Part 2: Probes*, Standard EN 12668-2:2010, 2010.

[7] K. A. Wear and Y. Liu, "Considerations for choosing sensitive element size for needle and fiber-optic hydrophones—Part II: Experimental validation of spatial averaging model," *IEEE Trans. Ultrason., Ferroelectr., Freq. Control*, vol. 66, no. 2, pp. 340–347, Feb. 2019, doi: 10.1109/TUFFC.2018.2886071.

[8] K. A. Wear, C. Baker, and P. Miloro, "Directivity and frequency-dependent effective sensitive element size of needle hydrophones: Predictions from four theoretical forms compared with measurements," *IEEE Trans. Ultrason., Ferroelectr., Freq. Control*, vol. 65, no. 10, pp. 1781–1788, Oct. 2018, doi: 10.1109/TUFFC.2018.2855967.

[9] K. A. Wear and S. M. Howard, "Directivity and frequency-dependent effective sensitive element size of a reflectance-based fiber-optic hydrophone: Predictions from theoretical models compared with measurements," *IEEE Trans. Ultrason., Ferroelectr., Freq. Control*, vol. 65, no. 12, pp. 2343–2348, Dec. 2018, doi: 10.1109/TUFFC.2018.2872840.

[10] S. J. Sanabria, T. Marhenke, R. Furrer, and J. Neuenschwander, "Calculation of volumetric sound field of pulsed air-coupled ultrasound transducers based on single-plane measurements," *IEEE Trans. Ultrason., Ferroelectr., Freq. Control*, vol. 65, no. 1, pp. 72–84, Jan. 2018, doi: 10.1109/TUFFC.2017.2773619.

[11] W. Cui, R. N. Miles, and Q. Su, "A robust miniature silicon microphone diaphragm," *Sensors Transducers J.*, vol. 7, pp. 63–77, Oct. 2009.

[12] W. Galbraith and G. Hayward, "Development of a PVDF membrane hydrophone for use in air-coupled ultrasonic transducer calibration," *IEEE Trans. Ultrason., Ferroelectr., Freq. Control*, vol. 45, no. 6, pp. 1549–1558, Nov. 1998, doi: 10.1109/58.738294.

[13] A. G. Bashford, D. W. Schindel, D. A. Hutchins, and W. M. D. Wright, "Field characterization of an air-coupled micromachined ultrasonic capacitance transducer," *J. Acoust. Soc. Amer.*, vol. 101, no. 1, pp. 315–322, Jan. 1997, doi: 10.1121/1.418011.

[14] W. Westerveld, "Silicon photonic micro-ring resonators to sense strain and ultrasound," Ph.D. thesis, Dept. Imag. Phys., Faculty Applied Sciences, Delft Univ. Technol., Delft, The Netherlands, 2014.

[15] K. Chen et al., "Fiber-optic Fabry–Pérot interferometer based high sensitive cantilever microphone," *Sens. Actuator A, Phys.*, vol. 279, pp. 107–112, Aug. 2018, doi: 10.1016/j.sna.2018.06.010.

[16] S. Liao, T. Wong, Z. Wang, R. Wang, E. Clutter, and H.-T. Chien, "Miniature fiber laser microphones with graphene diaphragms," in *Proc. IEEE Res. Appl. Photon. Defense Conf. (RAPID)*, Aug. 2018, pp. 197–200.

[17] *Fibre-Optic Hydrophone Systems (FOHS) V2*, Precision Acoustics, Dorchester, U.K., 2022.

[18] W. Rohringer, T. Heine, R. Sommerhuber, N. Lehmann, and B. Fischer, "Optical microphone as laser-ultrasound detector," in *Proc. DAGA*, 2018, pp. 1–4.

[19] J. C. Grager et al., "Advances in air-coupled ultrasonic testing combining an optical microphone with novel transmitter concepts," in *Proc. ECNDT*, 2018, pp. 1–10.

[20] M. Almqvist, A. Holm, H. W. Persson, and K. Lindstrom, "Characterization of air-coupled ultrasound transducers in the frequency range 40 kHz–2 MHz using light diffraction tomography," *Ultrasonics*, vol. 37, no. 8, pp. 565–575, Jan. 2000, doi: 10.1016/S0041-624X(99)00168-7.

[21] L. Wang, W. Zhu, Z. Wu, W. Liu, and C. Sun, "A novel coupled piezoelectric micromachined ultrasonic transducer based on piston mode," *IEEE Trans. Ultrason., Ferroelectr., Freq. Control*, vol. 68, no. 11, pp. 3396–3405, Nov. 2021, doi: 10.1109/TUFFC.2021.3090043.

[22] A. Neild, D. A. Hutchins, T. J. Robertson, L. A. J. Davis, and D. R. Billson, "The radiated fields of focussing air-coupled ultrasonic phased arrays," *Ultrasonics*, vol. 43, no. 3, pp. 183–195, Jan. 2005, doi: 10.1016/j.ultras.2004.04.006.

[23] S. A. Zawawi, A. A. Hamzah, B. Y. Majlis, and F. Mohd-Yasin, "A review of MEMS capacitive microphones," *Micromachines*, vol. 11, no. 5, p. 484, May 2020, doi: 10.3390/mi11050484.

[24] T. Ling, S.-L. Chen, and L. J. Guo, "High-sensitivity and wide-directivity ultrasound detection using high q polymer microring resonators," *Appl. Phys. Lett.*, vol. 98, no. 20, May 2011, Art. no. 204103, doi: 10.1063/1.3589971.

[25] S. D. Wang, Y. C. Chen, S. C. Lo, Y. J. Wang, M. C. Wu, and W. L. Fang, "On the performance enhancement of cantilever diaphragm piezoelectric microphone," *IEEE Sensors*, Oct. 2021, pp. 1–4, doi: 10.1109/SENSORS47087.2021.9639769.

[26] S. Basiri-Esfahani, A. Armin, S. Forstner, and W. P. Bowen, "Precision ultrasound sensing on a chip," *Nature Commun.*, vol. 10, no. 1, p. 132, Jan. 2019, doi: 10.1038/s41467-018-08038-4.

[27] G. Caliano, V. Foglietti, E. Cianci, and M. Pappalardo, "A silicon microfabricated electrostatic transducer: 1 MHz transmission in air and in water," *Microelectron. Eng.*, vol. 53, nos. 1–4, 573-576, pp. Jun. 2000, doi: 10.1016/S0167-9317(00)00381-6.

[28] S. Rupitsch, R. Lerch, J. Strobel, and A. Streicher, "Ultrasound transducers based on ferroelectret materials," *IEEE Trans. Dielectr. Electr. Insul.*, vol. 18, no. 1, pp. 69–80, Feb. 2011, doi: 10.1109/TDEI.2011.5704495.

[29] J. L. Ealo, F. Seco, and A. R. Jimenez, "Broadband EMFi-based transducers for ultrasonic air applications," *IEEE Trans. Ultrason., Ferroelectr., Freq. Control*, vol. 55, no. 4, pp. 919–929, Apr. 2008, doi: 10.1109/TUFFC.2008.727.

[30] I. Graz et al., "Flexible ferroelectret field-effect transistor for large-area sensor skins and microphones," *Appl. Phys. Lett.*, vol. 89, no. 7, Aug. 2006, Art. no. 073501, doi: 10.1063/1.2335838.

[31] V. Bovtun, J. Doring, J. Bartusch, U. Beck, A. Erhard, and Y. Yakymenko, "EMFIT ferroelectret film transducers for non-contact ultrasonic testing," in *Proc. ECNDT*, 2006, pp. 1–10.

[32] J. Q. Aguilar, M. Munoz, and T. G. Alvarez-Arenas, "Interpretation of the thickness resonances in ferroelectret films based on a layered sandwich mesostructure and a cellular microstructure," *IEEE Trans. Ultrason., Ferroelectr., Freq. Control*, vol. 68, no. 4, pp. 1245–1252, Apr. 2021, doi: 10.1109/TUFFC.2020.3025358.

[33] J. Quirce, L. Svilainis, J. Camacho, and T. G. Alvarez-Arenas, "Ferroelectret ultrasonic transducers for pulse-echo water immersion," *Appl. Sci.*, vol. 10, no. 24, p. 8771, Dec. 2020, doi: 10.3390/app10248771.

[34] J. Hillenbrand and G. M. Sessler, "DC-biased ferroelectrets with large piezoelectric d_{33}-coefficients," *J. Appl. Phys.*, vol. 103, no. 7, Apr. 2008, Art. no. 074103.

[35] X. Zhang, J. Hillenbrand, and G. M. Sessler, "Improvement of piezoelectric activity of cellular polymers using a double-expansion process," *J. Phys. D, Appl. Phys.*, vol. 37, no. 15, pp. 2146–2150, Aug. 2004, doi: 10.1088/0022-3727/37/15/015.

[36] J. Hillenbrand and G. M. Sessler, "High-sensitivity piezoelectric microphones based on stacked cellular polymer films (L)," *J. Acoust. Soc. Amer.*, vol. 116, no. 6, pp. 3267–3270, Dec. 2004, doi: 10.1121/1.1810272.

[37] J. Hillenbrand and G. M. Sessler, "Piezoelectret microphones with high sensitivity," in *Proc. 12th Int. Symp. Electrets*, 2005, pp. 125–128.

[38] V. Bovtun et al., "Air-coupled ultrasonic applications of ferroelectrets," *Ferroelectrics*, vol. 370, pp. 11–17, Oct. 2008, doi: 10.1080/00150190802380243.

[39] *Ultrasonic Applications for Knowles Electret and MEMS Microphones*, Knowles Electronics, Bengaluru, India, 2013.

[40] T. E. Gómez Álvarez-Arenas, H. Calás, J. E. Cuello, A. R. Fernández, and M. Muñoz, "Noncontact ultrasonic spectroscopy applied to the study of polypropylene ferroelectrets," *J. Appl. Phys.*, vol. 108, no. 7, Oct. 2010, Art. no. 074110, doi: 10.1063/1.3490788.

[41] L. Svilainis, V. Dumbrava, and D. Kybartas, "Evaluation of the ultrasonic preamplifier noise voltage density," *J. Circuits, Syst. Comput.*, vol. 23, no. 1, Jan. 2014, Art. no. 1450007, doi: 10.1142/S0218126614500078.

[42] L. Svilainis, D. Kybartas, A. Aleksandrovas, and T. E. G. Alvarez-Arenas, "High frequency focused imaging for ultrasonic probe integrity inspection," *NDT & E Int.*, vol. 116, Dec. 2020, Art. no. 102360, doi: 10.1016/j.ndteint.2020.102360.

[43] L. Svilainis, A. Chaziachmetovas, D. Kybartas, and T. G. Alvarez-Arenas, "Air-coupled ultrasonic probe integrity test using a focused transducer with similar frequency and limited aperture for contrast enhancement," *Sensors*, vol. 20, no. 24, p. 7196, Dec. 2020, doi: 10.3390/s20247196.

[44] J. P. Monchalin, "Laser-ultrasonics: Principles and industrial applications," *E-J. Nondestruct. Test.*, vol. 3, pp. 1–43, Jan. 2020.

[45] S. Dixon, T. Harrison, Y. Fan, and P. A. Petcher, "Thermoelastic laser generated ultrasound using a ring source," *J. Phys. D, Appl. Phys.*, vol. 45, no. 17, May 2012, Art. no. 175103, doi: 10.1088/0022-3727/45/17/175103.

[46] L. F. Bresse and D. A. Hutchins, "Transient generation by a wide thermoelastic source at a solid surface," *J. Appl. Phys.*, vol. 65, pp. 1441–1449, Feb. 1989, doi: 10.1063/1.342956.

[47] C. B. Scruby, H. N. G. Wadley, R. J. Dewhurst, S. B. Palmer, and D. A. Hutchins, "A laser-generated standard acoustic emission source," *Mater. Eval.*, vol. 39, pp. 1250–1254, Dec. 1981.

[48] L. Svilainis, A. Chaziachmetovas, V. Eidukynas, A. Aleksandrovas, and M. Varatinskas, "Compact laser driver for ultrasonic arbitrary position and width pulse sequences generation," *IEEE Trans. Instrum. Meas.*, vol. 70, pp. 1–15, 2021, doi: 10.1109/TIM.2021.3120144.

[49] V. V. Krylov, "Directivity patterns of laser-generated sound in solids: Effects of optical and thermal parameters," *Ultrasonics*, vol. 69, pp. 279–284, Jul. 2016, doi: 10.1016/j.ultras.2016.01.011.

[50] F. Gao et al., "An analytical study of photoacoustic and thermoacoustic generation efficiency towards contrast agent and film design optimization," *Photoacoustics*, vol. 7, pp. 1–11, Sep. 2017, doi: 10.1016/j.pacs.2017.05.001.

[51] M. N. Hasan, M.-U. Haque, and Y. C. Lee, "Deastigmatism, circularization, and focusing of a laser diode beam using a single biconvex microlens," *Opt. Eng.*, vol. 55, no. 9, Sep. 2016, Art. no. 095107, doi: 10.1117/1.OE.55.9.095107.

[52] M. Serkan and H. Kirkici, "Reshaping of a divergent elliptical Gaussian laser beam into a circular, collimated, and uniform beam with aspherical lens design," *IEEE Sensors J.*, vol. 9, no. 1, pp. 36–44, Jan. 2009, doi: 10.1109/JSEN.2008.2008882.

[53] X. Q. Zhou, B. K. A. Ngoi, and S. S. Koh, "Single aspherical lens for deastigmatism, collimation, and circularization of a laser beam," *Appl. Opt.*, vol. 39, no. 7, pp. 1148–1151, Mar. 2000.

[54] M. Erfanzadeh, P. D. Kumavor, and Q. Zhu, "Laser scanning laser diode photoacoustic microscopy system," *Photoacoustics*, vol. 9, pp. 1–9, Mar. 2018, doi: 10.1016/j.pacs.2017.10.001.

[55] A. Hariri et al., "Development of low-cost photoacoustic imaging systems using very low-energy pulsed laser diodes," *J. Biomed. Opt.*, vol. 22, no. 7, Jul. 2017, Art. no. 075001, doi: 10.1117/1.JBO.22.7.075001.

[56] V. Dumbrava and L. Svilainis, "The automated complex impedance measurement system," *Elektron. Elektrotech.*, vol. 76, no. 4, pp. 59–62, Jan. 2007.

[57] L. Svilainis, V. Dumbrava, S. Kitov, A. Aleksandrovas, P. Tervydis, and D. Liaukonis, "Electronics for ultrasonic imaging system," *Elektronika Elektrotechnika*, vol. 20, no. 7, pp. 51–56, Sep. 2014, doi: 10.5755/j01.eee.20.7.8024.

[58] Y. Wang, M. Sun, Y. Cao, and J. Zhu, "Application of optical interferometry in focused acoustic field measurement," *J. Sound Vib.*, vol. 426, pp. 234–243, Jul. 2018, doi: 10.1016/j.jsv.2018.04.023.

[59] L. Svilainis, A. Chaziachmetovas, and T. E. G. Alvarez-Arenas, "Ultrasonic needle hydrophone calibration in air by parabolic off-axis mirror focused beam using three-transducer reciprocity," to be published.

[60] D. A. Hutchins, R. J. Dewhurst, and S. B. Palmer, "Laser generated ultrasound at modified metal surfaces," *Ultrasonics*, vol. 19, no. 103, pp. 103–108, May 1981, doi: 10.1016/0041-624X(81)90078-0.

[61] C. Edwards, T. Stratoudaki, and S. B. Palmer, "A new thermoelastic source model for non-metals," in *Proc. RPQNE*, vol. 22, 2003, pp. 326–332.

[62] J. Wang, B. Xu, Z. Shen, X. Ni, and J. Lu, "Influence of transparent coating thickness on thermoelastic force source and laser-generated ultrasound waves," *Appl. Surf. Sci.*, vol. 255, no. 16, pp. 7172–7178, May 2009, doi: 10.1016/j.apsusc.2009.03.054.

[63] *Ultrasonics—Hydrophones—Part 3: Properties of Hydrophones for Ultrasonic Fields up to 40 MHz*, Standard IEC 62127-3:2007, 2007.

[64] T. E. G. Alvarez-Arenas, "Air-coupled piezoelectric transducers with active polypropylene foam matching layers," *Sensors*, vol. 13, no. 5, pp. 5996–6013, 2013, doi: 10.3390/s130505996.

[65] L. Gaete-Garreton, J. A. Gallego-Juárez, and E. Riera, "Nonlinear problems in the generation, propagation and measurement of high intensity ultrasonic waves in air," in *Proc. Meetings Acoust. 6ICU*, vol. 32, 2017, Art. no. 045027, doi: 10.1121/2.0000782.

[66] A. Selfridge and P. A. Lewin, "Wideband spherically focused PVDF acoustic sources for calibration of ultrasound hydrophone probes," *IEEE Trans. Ultrason., Ferroelectr., Freq. Control*, vol. 47, no. 6, pp. 1372–1376, Nov. 2000, doi: 10.1109/58.883526.
[67] *Underwater Acoustics—Hydrophones—Calibration of Hydrophones—Part 1: Procedures for Free-Field Calibration of Hydrophones*, Standard IEC 60565-1:2020, 2020.
[68] L. Svilainis, A. Chaziachmetovas, and V. Dumbrava, "Half bridge topology 500 V pulser for ultrasonic transducer excitation," *Ultrasonics*, vol. 59, pp. 79–85, May 2015, doi: 10.1016/j.ultras.2015.01.014.
[69] T. D. Mast and F. Yu, "Simplified expansions for radiation from a baffled circular piston," *J. Acoust. Soc. Amer.*, vol. 118, no. 6, pp. 3457–3464, Dec. 2005, doi: 10.1121/1.2108997.
[70] D. A. Hutchins, T. J. Robertson, and D. R. Billson, "New designs of focused air-coupled ultrasonic transducer," *Revista Acustica*, vol. 33, pp. 3–4, Jan. 2002.
[71] T. E. G. Álvarez-Arenas, J. Camacho, and C. Fritsch, "Passive focusing techniques for piezoelectric air-coupled ultrasonic transducers," *Ultrasonics*, vol. 67, pp. 85–93, Apr. 2016, doi: 10.1016/j.ultras.2016.01.001.

Linas Svilainis (Senior Member, IEEE) received the Ph.D. degree from the Kaunas University of Technology, Kaunas, Lithuania, in 1996.

Since 2009, he has been a full-time Professor with the Department of Electronics Engineering, Kaunas University of Technology, where he is currently a Principal Investigator of the Signal Technologies Group. His current research interests include design and optimization of ultrasound electronics, ultrasonic signal processing, large-scale LED video displays, and electromagnetic compatibility and electromagnetic interference (EMI) protection of electronic systems.

Andrius Chaziachmetovas (Member, IEEE) received the Ph.D. degree in metrology and measurements from the Kaunas University of Technology, Kaunas, Lithuania, in 2007.

Since 2009, he has been an Associate Professor with the Department of Electronics Engineering, Kaunas University of Technology, Kaunas. His current research interests include ultrasonic measurements, ultrasound electronics, high-voltage pulsers, software development, embedded systems, and time of flight estimation.

Valdas Eidukynas received the Ph.D. degree from the Kaunas University of Technology, Kaunas, Lithuania, in 1996.

Since 2019, he has been a full-time Professor with the Department of Mechanical Engineering and Design, Kaunas University of Technology. His current research interests include computer-aided modeling and numerical analysis methods and tools in static and dynamic analysis of solid bodies and fluid–structure interaction under the static, dynamic, seismic, and thermal loading.

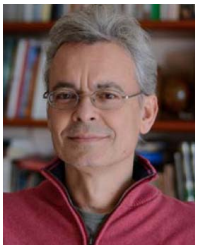

Tomás Gómez Álvarez-Arenas (Member, IEEE) received the Ph.D. degree in physics from the Complutense University of Madrid, Madrid, Spain, in 1994.

In 1996, he joined the Center for Ultrasonic Engineering, Strathclyde University, Glasgow, U.K., as a Postdoctoral Researcher. In 2000, he joined the Institute of Acoustics, Spanish National Research Council (CSIC), Madrid, and then the Institute of Physical and Information Technologies (ITEFI), CSIC, in 2013. Since 2014, he has been the Head of the Sensors and Ultrasonic Technologies Department, ITEFI, CSIC. His research interests include design, optimization, and fabrication of piezoelectric transducers; the study of piezoelectric and ferroelectric materials; ultrasonic materials characterization; new materials for ultrasonic applications; solution of inverse and hard optimization problems; and applications of ultrasonic techniques in non-destructive testing (NDT), medical diagnosis, food quality, industrial control, and agriculture sensing.

Steve Dixon is currently the Director of the Centre for Industrial Ultrasonics (CIU), University of Warwick, Coventry, U.K. He has involved in the area of ultrasonics for 30 years and has authored or coauthored over 150 peer-reviewed journal articles. His research interests include ultrasonic measurements of material properties, noncontact ultrasound, nondestructive evaluation and testing, ultrasonic transduction, ultrasonic measurement of metallurgical microstructure, eddy current and electromagnetic inspection, and thermographic non-destructive testing (NDT).

Prof. Dixon is a Co-Founding Member of the U.K. Research Centre for NDE (RCNDE). He has held four research fellowships.